Kinetic modeling of the thermal degradation and combustion of biomass

Eliseo Ranzi *, Michele Corbetta, Flavio Manenti, Sauro Pierucci

Politecnico di Milano, Dipartimento di Chimica, Materiali e Ingegneria Chimica "Giulio Natta", Piazza Leonardo da Vinci 32, 20133 Milano, Italy

Article history:
Received 15 April 2013
Received in revised form
20 June 2013
Accepted 8 August 2013

1. Introduction

Biomass is one of the most promising feedstocks able to satisfy the increasing demand for renewable energy and green chemicals. Unfortunately, biomass conversion is tough to be industrially scaled-up due to complexity of chemical and transport phenomena and research efforts are devoted to achieve a deeper insight in order to develop reliable comprehensive models. Mechanistic models capable of describing transport phenomena and reaction kinetics are the critical step towards a better understanding of biomass pyrolysis. Detailed chemical mechanisms are needed, both for biomass pyrolysis and for the successive gas phase reactions, since they would lead to accurate process optimization, but they are still unavailable even for major products released such as levoglucosan (LVG), hydroxymethylfurfural (HMFU), and phenolic species. Chemical mechanisms need to be integrated into particle model accounting for transport phenomena, which are critical in predicting the global reactor performance. Developing these models is challenging because of the biomass complexity as well as the multi-phase and multi-scale nature of the conversion process (Mettler et al., 2012).

* Corresponding author. Tel.: +39 02 2399 3250; fax: +39 02 7063 8173.
E-mail address: eliseo.ranzi@polimi.it (E. Ranzi).

Combustion, gasification, and biomass-to-liquid pyrolysis are some of the main thermo-chemical conversion routes, which can convert an abundant and well distributed feedstock into energy, syngas, bio-oil, and chemicals. One of the main problems when studying this type of feedstock is the intrinsic variability of the biomass composition. As a consequence, it is necessary to properly characterize the biomass, preferably on the basis of few lumped components, which are typical for all the possible feedstocks.

The kinetic model here proposed is an extension of the previous one (Ranzi et al., 2008) and is based on a multi-step devolatilization and decomposition of the three key-biomass reference species: cellulose, hemicelluloses and lignin. One of the main features of this model is its ability to provide detailed information on yields composition of gas, tar, and solid residue. This revision and extension of the previous model was obtained taking advantage of the recent literature and through several comparisons between model predictions and experimental data. The kinetic model also involves the char gasification and combustion reactions, with steam and/or air or oxygen, as well as the secondary homogeneous gas phase reactions of the released gas and tar species. The multistep kinetic model was originally validated on the basis of thermo-gravimetric data of fine particles, with negligible resistances. The first three application examples of the ones proposed later in the paper, at the particle scale, emphasize the effect of the coupling of reaction kinetics with mass and heat transfer resistances. In accordance with the adopted multi-scale approach, the examples at the particle scale will be extended to the reactor scale with the analysis of a biomass gasifier and a traveling grate biomass combustor. It is important to underline that the main goal of this paper is to provide an overall view of our recent works on modeling biomass pyrolysis, gasification, and combustion. More than the direct comparisons with experimental data, the aim of the quoted application results is to show the possibilities as well as the limitations of the adopted lumped approach. Several examples have been already presented and discussed in previous papers (Gauthier et al., 2013; Pierucci and Ranzi, 2008; Ranzi et al., 2011; Sommariva et al., 2011). Meanwhile, the kinetic model of biomass pyrolysis has been progressively modified in order to continuously account for new available experimental data. For instance, recent modifications of the kinetic scheme refer to reaction heats. New experimental data on the center temperature profiles of thick biomass particles, recently obtained at CEA Grenoble (Gauthier et al., 2013), allowed to better investigate the thermochemistry of volatilization and charification processes. Moreover, the low temperature experimental activities on biochar formation (Bennadji et al., 2012), with detailed time resolved species concentration profiles, allowed to further tune and modify the overall stoichiometries. All these modifications were made without relevant effects on previous validations. The same approach has been and is still adopted to extend the secondary gas-phase kinetic scheme (http://creckmodeling.chem.polimi.it/). Thus, the pioneering kinetic work on hydrocarbon pyrolysis (Dente et al., 1979) was first applied to the oxidation and combustion of hydrocarbon fuels (Ranzi et al., 1994) and it is also nowadays extended to new oxygenated components, such as furans of relevant interest as biofuels (Saggese et al., 2013).

The paper is thereby structured as follows. The biomass characterization by means of reference components is presented in Section 2. The same section describes the multi-step nature of the kinetic model together with the heterogeneous reactions of char gasification and combustion as well as the secondary gas-phase reactions. The kinetic model is then involved in the balance equations at the particle and reactor level highlighting the multi-scale nature of this problem. Mass and energy balances are given in Section 3. The application examples are discussed in Section 4. Applications cover all the scales: the temperature overshooting of the center of a biomass particle; the effective start-up procedure to achieve the desired steady-state conditions of a single layer of a biomass bed; a third example, always at the particle scale, analyses the possibility to reach gasification or combustion regimes, depending on the relative role of reaction kinetics and thermal resistances; finally, the temperature profiles in a countercurrent biomass gasifier, and the parametric sensitivity for control purposes of a traveling grate biomass combustor constitute a couple of examples demonstrating the viability as well as the limitations of the proposed approach. At last, numerical methods and the structure of the Jacobian matrix of the resulting algebraic-differential system are discussed in Appendix A.

2. Biomass characterization and multi-step kinetic model

2.1. Biomass characterization

It is well known that cellulose (40–50 wt%), hemicellulose (25–35 wt%) and lignin (15–35 wt%) are the building blocks of woody biomass (Vinu and Broadbelt, 2012). Accordingly, the present multi-step kinetic model characterizes the biomass as a mixture of these three major components, together with moisture and inert ashes. In addition, lignin is further detailed as a combination of three reference components with different methoxylation degree, LIGH, LIGO, and LIGC, which are richer in hydrogen, oxygen and carbon, respectively (Faravelli et al., 2010). A very similar approach is also used by the chemical percolation devolatilization (bio-CPD) model assuming that biomass pyrolysis occurs as a weighted average of its individual components (cellulose, hemicellulose, and lignin). The char, tar, and light gas yields of a particular biomass are then calculated as the weighted average of the pyrolysis yields of these three components (Lewis and Fletcher, 2013). It is worth underlining that the effect of extractives on the mechanism of biomass pyrolysis is not specifically addressed in this model, even though it is known that biomass extractives can catalyze or alter the reactions occurring during biomass pyrolysis.

Usually, biochemical analysis of biomass is unavailable and a method to characterize the biomass feedstock on the basis of the bare elemental analysis has been proposed elsewhere (Ranzi et al., 2008). If only the elemental analysis in terms of C, H, and O content is available, then a suitable combination of the reference species is simply derived from the three atomic balances. For this reason three mixtures of the reference components (cellulose, hemicellulose, and lignin) are proposed, and the biomass feedstock is characterized as a linear combination of these reference mixtures. The first is a molar mixture of 60% cellulose and 40% hemicellulose, while the remaining ones are mixtures of the kinds of lignins (80% LIGO+20% LIGC, and 80% LIGH+20% LIGC). An example of this procedure is provided in Fig. 1, in which the three reference mixtures are reported on the H/C diagram as black filled circles, and a typical biomass feedstock as a black diamond. The biomass is then characterized as a linear combination of the three reference mixtures at the vertices of the triangle, and it is subject to the atomic balance constraints. Clearly, whenever the selected reference mixtures are unable to properly characterize certain biomass samples with high contents in hydrogen, oxygen or carbon, they can be accordingly modified to include these less common samples.

2.2. Multi-step kinetic model of biomass pyrolysis

A very large detail of the released products from biomass pyrolysis was recently reported by Weng et al. (2013). They studied the pyrolysis process of poplar biomass with tunable synchrotron vacuum ultraviolet photoionization mass spectrometry (PIMS) and they were able to measure the time-evolved profiles of several species during the pyrolysis process. Moreover,

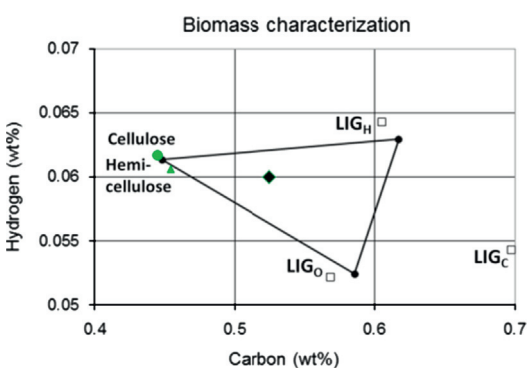

Weight fraction of reference components:

(daf basis)		
Cellulose	- $C_6H_{10}O_5$-	0.329
Hemicellulose	- $C_5H_8O_4$-	0.179
LIGH	- $C_{22}H_{28}O_9$-	0.253
LIGO	- $C_{20}H_{22}O_{10}$-	0.175
LIGC	- $C_{15}H_{14}O_4$-	0.064

Fig. 1. Biomass characterization using three reference components.

Vinu and Broadbelt (2012) developed a detailed and mechanistic kinetic model of pyrolysis of cellulose to predict the major bio-oil components (levoglucosan, formic acid, glyoxal, and furfural), besides several other minor products. This very detailed kinetic model was satisfactorily applied to the pyrolysis of other glucose-based carbohydrates. Similarly, Carstensen and Dean (2010) as well as Seshadri and Westmoreland (2012) investigated the implications of concerted molecular reactions for cellulose and hemicellulose kinetics. Even though this detailed description level seems too deep for the successive applications at the reactor scale, it is clear that all this information is very useful and contributes to the extension and to a better definition of stoichiometries of the global reactions of biomass pyrolysis (Ranzi et al., 2008).

Blondeau and Jeanmart (2012) have recently used this kinetic model and they also discussed some discrepancies between model predictions and experimental data of beech wood pyrolysis. On this and similar basis (Miller and Bellan, 1997) suggested some modifications to the mechanism in order to better predict gas and tar emissions. The apparent stoichiometry of the lumped reactions of biomass pyrolysis are thus modified taking advantage from these suggestions, from the predictions of more detailed kinetic models (Carstensen and Dean, 2010; Faravelli et al., 2010; Seshadri and Westmoreland, 2012; Vinu and Broadbelt, 2012) as well as from the already mentioned and recent experimental data (Bennadji et al., 2012; Weng et al., 2013). The revised version of the biomass pyrolysis model, including the reaction heats, is reported in Table 1 of the Supplementary material.

As far as the mechanism of cellulose is concerned, the heats of reaction agree with the observation by Milosavljevic et al. (1996). The tar release is an endothermic process, absorbing ~500 kJ/kg of volatiles produced, while the char formation is an exothermic reaction releasing ~2000 kJ/kg of char formed. The revised kinetic model, as well as these reaction heats, has been validated by comparing the model predictions to the experimental temperature profiles within several biomass samples acquired from the literature (Bennadji et al., 2012; Gauthier et al., 2013; Park et al., 2010). Results of these comparisons are presented and discussed later on the paper, showing a reasonable agreement between predicted and experimental data.

2.3. Heterogeneous reactions of char gasification and combustion

In thermally-thick particles, where the heating and reaction front moves from the external surface to the center of the particle, the char heterogeneous reactions are initially inhibited by the diffusion of volatile pyrolysis products (Williams et al., 2012). Similarly, char gasification and/or combustion reactions occur after the end of the biomass pyrolysis process, also in fine particles. The surface area and reactive properties of the residual char are related to the pyrolysis conditions and to the physical and chemical properties of the original biomass. Despite of the high porosity of the char, these reactions are usually the rate determining step in the overall gasification or combustion process. Table 2 in the Supplemental material summarizes the reference kinetic parameters of char combustion and gasification reactions (Groeneveld and Van Swaaij, 1980; Kashiwagi and Nambu, 1992; Tognotti et al., 1991).

2.4. Secondary gas-phase reactions

The secondary gas phase reactions of the released volatile species (tar and gas) are then described by using a general and detailed kinetic scheme of pyrolysis and combustion of hydrocarbon and oxygenated fuels (Ranzi et al., 2012). The complete kinetic model in CHEMKIN format together with thermodynamic properties of all involved species is available at the website: www.creckmodeling.chem.polimi.it. The number of species included in the gas-phase kinetic model is always a good compromise between the accuracy needed and the computational effort. For this reason, tar and heavy species are grouped into lumped or pseudo-components representative of isomers or analogous species with similar reactivity.

Very recently, Norinaga et al. (2013) developed a two-stage tubular reactor for evaluating the secondary reactions of the products from cellulose pyrolysis, while minimizing the interactions amongst char and volatile species. They investigated the pyrolysis system at a residence time of up to 6 s in a temperature range from 973 K to 1073 K. These new data constitute a further interesting test for the validation of the secondary gas-phase reactions. Fig. 2 shows a comparison of predicted and experimental yields of several species. CO is the most abundant product, followed by major products such as H_2O, CH_4, and H_2. The model correctly predicts the secondary formation of CO, methane, H_2, ethylene, CO_2, and benzene, while mass fractions of propylene and oxygenated species (not reported) decrease over time.

3. Multi-scale modeling

Intra- and inter-phase heat and mass transfer phenomena need to be considered and coupled with the kinetics when modeling reactors treating thick particles. According to prior works (Pierucci and Ranzi, 2008; Ranzi et al., 2011), a convenient way to present the mass and energy balance equations is to distinguish the particle and the reactor scale.

3.1. Particle scale

The particle model should be able to predict temperature profiles and product distribution as a function of time. This model

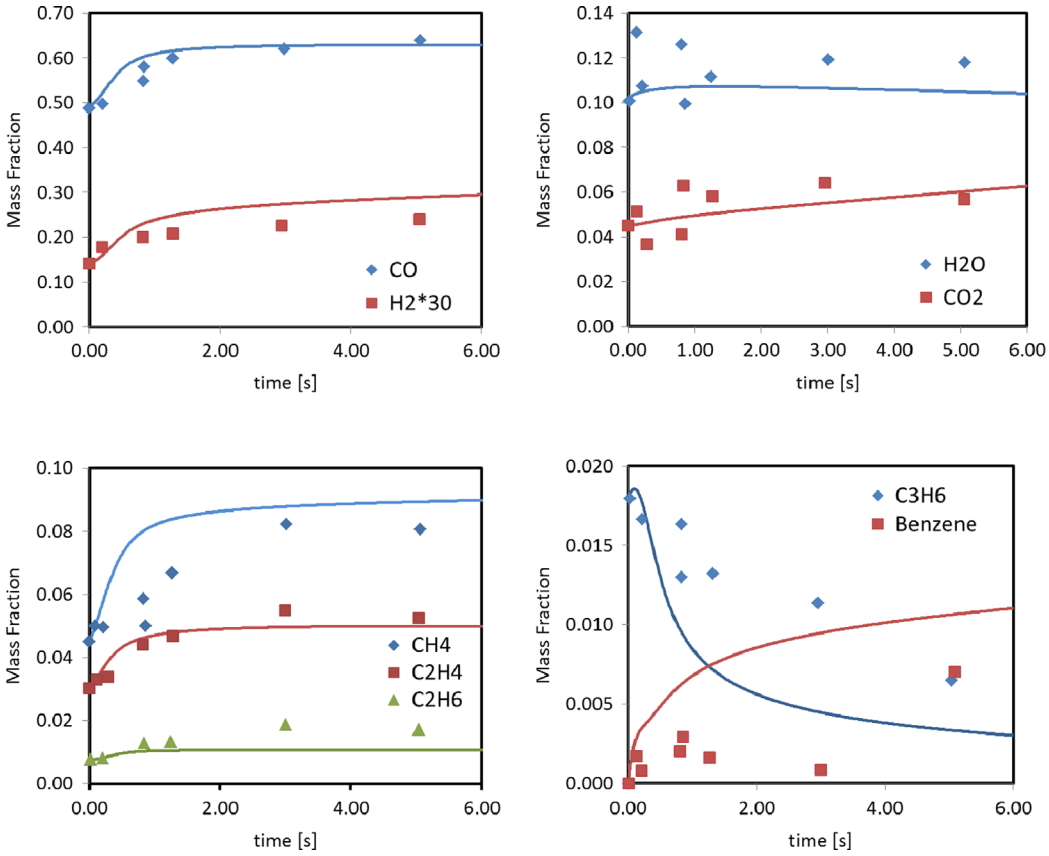

Fig. 2. Secondary pyrolysis of cellulose products at 1023 K. Comparison of predicted (solid lines) and experimental (symbols) yields of H_2, H_2O, CO, CO_2, methane, ethylene, ethane, propylene, and benzene (Norinaga et al., 2013).

requires not only reaction kinetics, but also reliable rules for estimating transport properties to account for morphological changes during the pyrolysis process. Biomass particles shrink by as much as 50% during their conversion. Heat transfer must account for variable transport properties during the pyrolysis process: namely, in virgin biomass, dry and reacting biomass, and the residual char (Di Blasi, 1993, 2008).

The intra-particle mass and heat transfer resistances are simply described by assuming an isotropic sphere. The particle is discretized into several sectors to characterize the temperature and concentration profiles, and the dynamic behavior of the particle under pyrolysis, gasification and combustion regimes. The gradients of temperature and volatile species inside the particle are evaluated by means of the energy and continuity equations, respectively. *N* sectors are assumed to discretize the particle.

The mass balance of the solid phase is:

$$\frac{dm_{j,i}}{dt} = V_j R_{j,i} \tag{1}$$

where $m_{j,i}$ is the mass of the *i*th solid component; V_j is the volume of the *j*th sector; $R_{j,i}$ is the net formation rate of the *i*th component resulting from the multi-step devolatilization model and from the heterogeneous gas–solid reactions in the *j*th sector; finally, *t* is the time variable.

The mass balance of the gas phase is:

$$\frac{dm_{j,i}}{dt} = J_{j-1,i}S_{j-1} - J_{j,i}S_j + V_j R_{j,i} \tag{2}$$

where $m_{j,i}$ is the mass of the *i*th volatile species within the *j*th sector; S_j is the external surface of the *j*th sector; and *J* is the total fluxes generated by diffusion and pressure gradients.

The energy balance is:

$$\frac{d\sum_{i=1}^{NCP} m_{j,i}h_{j,i}}{dt} = JC_{j-1}S_{j-1} - JC_jS_j + S_{j-1}\sum_{i=1}^{NCG} J_{j-1,i}h_{j-1,i} - S_j\sum_{i=1}^{NCG} J_{j,i}h_{j,i} + V_j HR_j \tag{3}$$

where $h_{j,i} = c_{P_{j,i}}T_j$ is the component partial enthalpy; T_j is the temperature of the *j*th sector. The term *JC* accounts for the heat conduction; the term $V \cdot HR$ accounts for the total reaction heat; *NCP* is the total number of components; and *NCG* is the number of gas components.

Mass exchange between adjacent sectors is only allowed for the volatile species, whereas solid compounds are constrained to remain inside the sector. The density profile inside the particle is evaluated as the sum of all the densities of different species $m_{j,i}$ present in each sector. Similarly, the shrinking and porosity of each sector are calculated. Mass and heat fluxes within the particle follow the constitutive Fick, Fourier, and Darcy laws:

$$J_{j,i} = -D_{j,i}^{eff} MW_i \left.\frac{dc_{j,i}}{dr}\right|_{r_j} - \left.\frac{Da_j dP_j}{\mu_j\, dr}\right|_{r_j} c_{j,i}MW_i \tag{4}$$

where $D_{j,i}^{eff}$ is the effective diffusion coefficient of the *i*-th component inside the *j*th sector; *MW* and *c* are the molecular weight and the concentration; *r* is the radius; *Da* is the Darcy coefficient of the solid; μ is the viscosity of the gas phase; *P* is the pressure.

$$JC_j = -\kappa_j^{eff} \left.\frac{dT_j}{dr}\right|_{r_j} \tag{5}$$

where κ_j^{eff} is the effective conduction coefficient inside the *j*th sector.

The boundary conditions at the gas–solid interface become:

$$J_{N,i} = k_{ext} MW_i (c_{N,i} - c_i^{bulk}) + \frac{Da_N \Delta P}{\mu_N \Delta r}\Big|_N c_{N,i} MW_i \tag{6}$$

$$JC_N = h_{ext}(T_N - T^{bulk}) + JR_N + \sum_i^{NCG} J_{N,i} h_{N,i} \tag{7}$$

where k_{ext} and h_{ext} are the convective transfer coefficients (Ranz and Marshall, 1952) and JR_N is the net radiation heat.

3.2. Reactor scale

While the mathematical model of fluidized bed or entrained bed reactors can directly refer to the previous particle model, the modeling of fixed bed reactors takes advantage from the definition of an elemental reactor layer describing the gas–solid interactions. The solid bed is then simulated as a series of *NR* elemental layers, as reported in Fig. 3. The height of each layer is of the same order of the size of the biomass particle, accounting for the vertical dispersion phenomena. The complete mixing inside the layer both for the gas and solid phase is assumed. In fact, the mixing of the main gas flow is further increased because of the energy provided by the volatile species released from the particles during the biomass pyrolysis (Frigerio et al., 2008).

The gas-phase mass balance equations for each elemental reactor are:

$$\frac{dg_i}{dt} = G_{in,i} - G_{out,i} + J_{N,i} S_N \eta + V_R R_{g,i} \tag{8}$$

where g_i is the mass of the ith species within the reactor volume V_R; $G_{in,i}$ and $G_{out,i}$ are the inlet and outlet flowrate; $R_{g,i}$ is the net formation from gas-phase reactions; the term $J_{N,i}$ is the gas–solid mass exchange multiplied by the particle surface S_N and the number η of particles inside the layer.

The gas-phase energy balance equation for each elemental reactor is:

$$\frac{d\sum_{i=1}^{NCG} g_i h_{g_i}}{dt} = \sum_{i=1}^{NCG} G_{in,i} h_{g_{in,i}} - \sum_{i=1}^{NCG} G_{out,i} h_{g_i} + \sum_{i=1}^{NCG} J_{N,i} h_{N,i} S_N \eta + h_{ext}(T_N - T^{bulk}) S_N \eta + V_R HR_g \tag{9}$$

where $h_{g,i} = c_{P_i} T^{bulk}$; T^{bulk} is the gas-phase temperature; the terms $G \cdot h_g$ are the enthalpies of inlet and outlet flowrates; the term $J \cdot h$ is the enthalpy flux relating to the mass transfer of a single particle; finally HR_g is the overall heat of gas-phase reactions.

As a matter of simplicity, the reactor index (from 1 to NR) is not reported in the balance Eqs. (8) and (9). Fig. 3 highlights the interactions between adjacent reactor layers, while further boundary conditions and closure equations are needed to characterize different reactor configurations. Numerical methods and the structure of the Jacobian matrix are discussed in Appendix A.

4. Application examples

Hereinafter some application examples of biomass pyrolysis, gasification, and combustion are provided, both at the particle and reactor scale. The mathematical model will be first applied to the description of the temperature profiles during the pyrolysis of thick biomass particles, then to a single reactor layer showing the importance of a proper start-up procedure to achieve the desired ignited operating condition. A third example shows the possible presence of a combustion regime when the gasification of thick biomass particles is analyzed, emphasizing the need of a comprehensive model to foresee these conditions. Finally, two examples at the reactor scale will describe viable model applications to the simulation of an industrial-scale gasifier and a traveling-grate biomass combustor.

4.1. Overshooting of the internal temperature in thick biomass particles

The kinetic model of biomass pyrolysis can be applied to thermally thin particles, only in absence of internal gradients. On the contrary, when treating coarse or chipped biomass particles it is necessary to apply the more comprehensive and coupled heat and mass transfer and pyrolysis model. Park et al. (2010) recently studied the thermal decomposition of thick biomass particles at

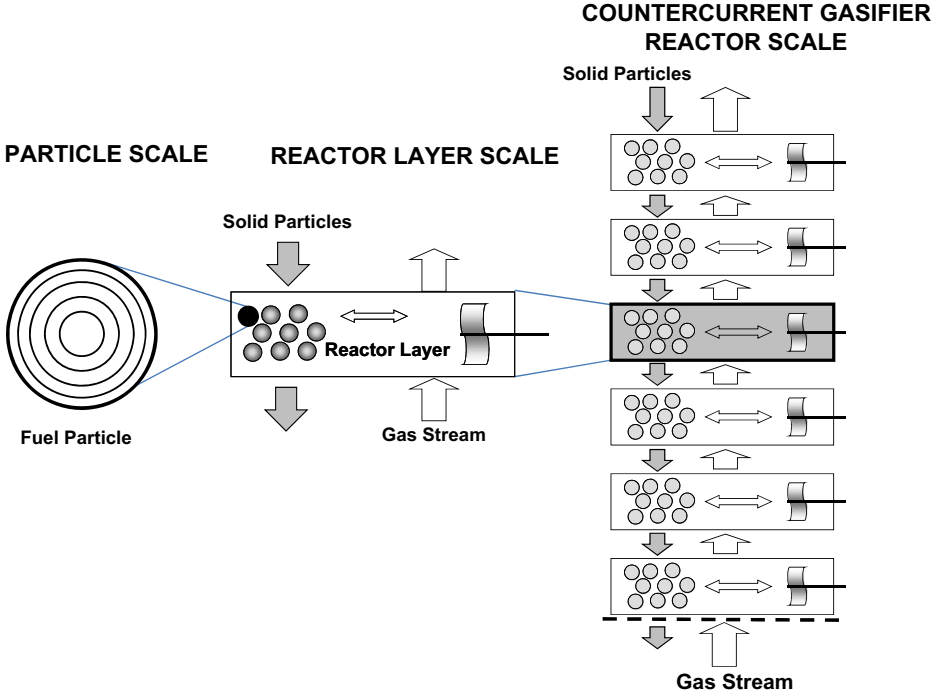

Fig. 3. Multi-scale structure of the countercurrent biomass gasifier of Section 4.4.

low temperatures, spanning from 638 K to 879 K. They measured the global mass losses, along with the temperature profiles at the surface and center of a spherical particle of 25.4 mm in diameter. The experimental results show a singular thermal behavior: after an initial increase of the core temperature, the temperature profile exhibits a plateau followed by a sharp peak, which overtakes the surface temperature profile. These temperature gradients are due to relevant thermal resistances. Biot number is very useful to evaluate the relative importance of external and internal heat transfer:

$$Bi = \frac{hd_p}{k_p} = Nu\frac{k_g}{k_p} \tag{10}$$

where h is the external heat-transfer coefficient; k_p and k_g are the biomass and gas thermal conductivity; and Nu is the Nusselt number. d_p is the equivalent spherical diameter of the particles:

$$d_p = \frac{6V_p}{S_p} \tag{11}$$

with V_p and S_p being the particle volume and surface, respectively. Large external heating rates and low thermal conductivity determine large Biot numbers for thick particles, causing the presence of temperature gradients within the particle. Values greater than 1 are typically obtained for particles larger than 0.2–0.3 mm in diameter. To evaluate the gradients of temperature, biomass composition, and gas concentrations both inside and outside the particle, it is necessary to solve the corresponding balance equations at the particle scale with appropriate boundary conditions.

Fig. 4a compares the predicted and measured temperatures of the core of biomass particles during the pyrolysis experiments at 638 K, 688 K, 783 K, and 879 K (Park et al., 2010). The temperature first increases until achieving an inflexion point at 600–650 K, between 200 s and 500 s. After the plateau, the temperature increases even exceeding the steady-state values of the nominal temperatures. According to Lédé (2012) and limiting our focus on cellulose, the boiling point of levoglucosane (LVG) is 612 K and 854 K for cellobiosan. These values suggest that only LVG would rapidly vaporize at these temperatures, whilst the dimer is not particularly volatile. Fig. 4b compares the measured and predicted temperature profiles of the particle center and surface and the fraction of biomass residue from pyrolysis experiment at 688 K. This behavior clearly highlights the presence of two different thermal regimes. The first one is related to an endothermic stage that causes the temperature profile to get flat. The second one leads to the rising of the center temperature, which temporarily overcomes the surface temperature. Similar results were already discussed by Milosavljevic et al. (1996) in the study of the thermochemistry of cellulose pyrolysis. On the basis of several reliable experimental data, they concluded that the endothermicity of the process mainly reflects the latent heat requirement for vaporizing the tar products. The presence of the peak in the center temperature profile is due to the exothermic character of char formation. Thus, only the use of a coupled and comprehensive model is able to explain these experimental data. The comparisons in Fig. 4 show that the duration of the plateau region is underpredicted by the model. The behavior of these temperature profiles is highly sensitive to the thermochemical properties of the biomass pyrolysis, as well as to the relative content of cellulose, hemicellulose and different lignins. However, rather than an accurate fitting on specific operating conditions, the major interest of this biomass pyrolysis model relies on a general agreement with experimental data from different sources. In fact, the comparison with other recent experimental data (Bennadji et al., 2012; Gauthier et al., 2013) does not seem to confirm these under-predictions.

4.2. Start-up procedure and multiplicity of steady-state solutions

As already shown elsewhere (Sommariva et al., 2011), even the biomass gasification or combustion in a single reactor layer can exhibit multiple steady-state solutions, depending on the start-up procedure. Let's consider here thick cellulose particles fed into a single reactor layer countercurrent to an air stream with a fuel equivalent ratio of 3, which is typical of gasification process. Both the inlet streams enter at 300 K in a gasifier layer with a cross-sectional area of 1 m^2 and 0.1 m high. The dynamic evolution of the system could bring to an ignited or a cold steady-state solution, depending on the start-up policy. This is due to the typical thermal feedback occurring in autothermal reactors. In order to start up the system, an auxiliary fuel is used to heat up the inlet air stream at 1400 K, until the ignition of released volatiles is observed in the gas phase. The dynamics of gas and solid temperatures is analyzed in Fig. 5 and it shows that the steady-state condition could reach a hot or a cold solution, depending on the adopted start-up policies.

Solid particles need to be heated up in order to devolatilize, only then heat generation can occur from the ignition of the volatiles with the cold inlet air flow. That is why the heat has to be provided by the auxiliary fuel until the exothermic partial oxidation reactions allow the adequate heating of the solid phase. A feasible start-up procedure is to feed the preheated air stream until fuel particles reach a suitable temperature for the release of the pyrolysis products, with successive gas phase reactions. When these high-temperature operating conditions are achieved, it is

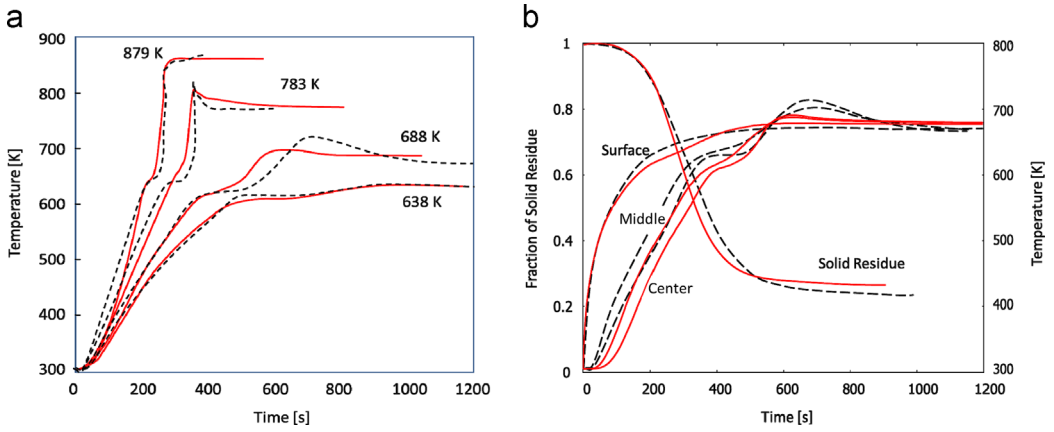

Fig. 4. Pyrolysis of a wood sphere. (a) Center temperature profiles. (b) Solid mass fraction and temperature profiles in a wood sphere at 688 K. Comparison between model predictions (solid lines) and experimental data (dashed lines) (Park et al., 2010).

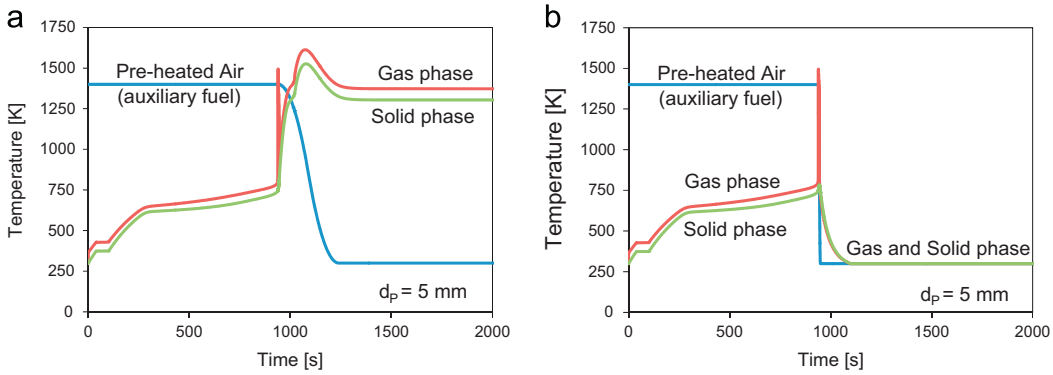

Fig. 5. Elemental gasification reactor. Dynamics of gas and solid temperature profiles to achieve a hot (a) and a cold (b) steady-state solution.

necessary to progressively reduce the inlet air temperature by preserving the hot condition, avoiding the system shutdown. Fig. 5 shows that it is not sufficient to simply observe the gas phase ignition. In fact, if the inlet air temperature is reduced too rapidly then the system is not anymore able to sustain the biomass pyrolysis and consequently there is a system shutdown, as shown in panel b of Fig. 5. On the contrary, the system is able to maintain the hot solution when the inlet air temperature is reduced more gradually. This is only a first example of the complexity related to the start-up and operations of the countercurrent gasifier, where multiple steady-state solutions could pertain to the different reactor layers.

4.3. Gasification and combustion regimes

The same configuration of the previous application example is here considered and the attention is focused on the gas–solid interactions. Different simulations are performed in order to highlight the influence of residence time on the gasification process, operated with wood particles (equivalent diameter of 3 cm) at equivalence ratio of 3. The progressive increase of the solid flow rate (i.e. the decrease of contact time) into the gasifier is analyzed. When the thermal penetration time ($\tau = \rho c_p d_p^2/k$) is higher than the residence time, the biomass particles are not uniformly heated.

Heat conduction is the controlling step for these thermally thick particles. As a consequence, only the external sectors pyrolyze, while the core of the particle remains at low temperatures. Fig. 6 shows the predicted gas and solid temperature profiles and the presence of two different regimes can be highlighted. At contact times higher than ~15 min, the gas phase temperature is lower than 1500 K, with small temperature gradients inside the particles. This is the behavior of the gasification regime. The biomass uniformly devolatilizes, char gasification is completed, and released gas and tar react with oxygen in the rich gas phase. Fuel equivalence ratio is 3, and the expected syngas with CO and H_2 is obtained. On the contrary, decreasing the residence time, the gas phase temperature increases to more than 2000 K. Internal temperature gradients become significant, the cold core of the particle remains unconverted. As a consequence, the biomass releases only partially the gas and tar species, leading to a fuel mixture approaching the stoichiometric conditions, with an effective equivalence ratio close to 1. This fact determines only a partial pyrolysis of the biomass particle and a nearly complete combustion of the released species, with large amounts of CO_2 and H_2O as final products. This becomes a typical surface combustion regime. After a further decrease of the residence time, the system is not anymore able to sustain the combustion regime, leading to the complete shutdown of the system. It is thus clear the need of

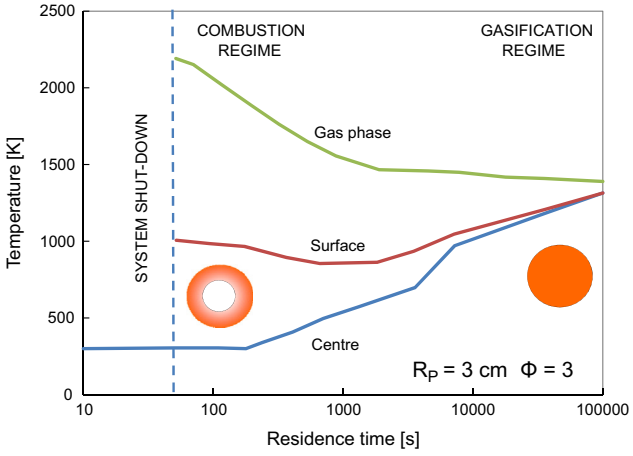

Fig. 6. Temperature profiles of the gas and solid phase as a function of the residence time in the reactor layer.

comprehensive models in order to analyze the behavior of these systems and to manage and/or optimize the operation of similar process units.

4.4. Countercurrent biomass gasifier

Fig. 7 schematically shows the countercurrent biomass gasifier. Biomass is fed continuously from the top, while the steam/air inlet stream enters the bottom of the gasifier. Air and oxygen amount is below the stoichiometric value, with an equivalence ratio of ~3, and the weight steam/biomass ratio is ~0.3. Gas contact time is in the order of few seconds, while the solid residence time is significantly higher and in the order of the hour. According to the multi-scale modeling approach, the whole countercurrent gasifier is analyzed by referring to a cascade of 10 reactor layers.

The resulting large and stiff DAE system, with several thousand equations, is very tough numerically. In fact, the nonlinearity of the system together with the possibility of multiple solutions, already emphasized in the previous examples, is further enhanced by the interconnections of the different layers. Accordingly, very effective and robust numerical methods and solvers are adopted (Buzzi-Ferraris and Manenti, 2010; Manenti et al., 2009).

Fig. 7 shows the vertical temperature profiles of the gas and solid phase, both center and surface temperatures are displayed. These profiles are reported according to the layer number, not to the real and steady shrink height. The effective volume of the first 5 layers, where the biomass and the residual char are completely converted, only contains ashes and is significantly reduced. At the bottom of the gasifier (layers 1–5) the gas and the solid temperatures are almost

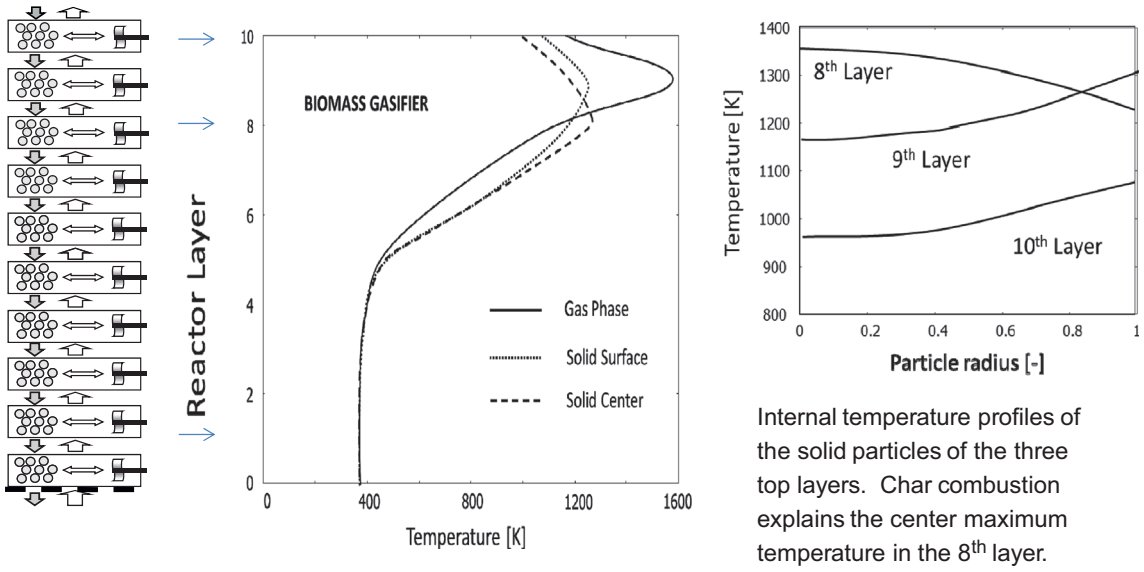

Fig. 7. Predicted temperature profiles in a countercurrent fixed bed biomass gasifier.

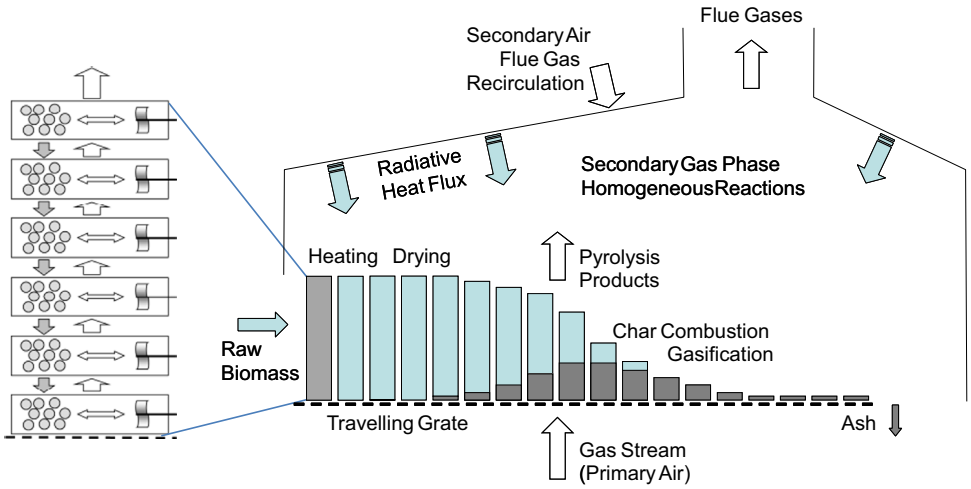

Fig. 8. Traveling grate biomass combustor.

similar. Rising the vertical direction of the bed, the gas is first heated up by the ash and the hot particles and then reaches more than 1500 K at the 8th–9th layers. In these layers, the exothermic partial oxidation reactions of tar products provide also the heat necessary to biomass devolatilization. The maximum temperature of the center of the particle in the 8th layer is due to the combustion of the residual char. Finally in the last reactor layer, the temperature of the gases leaving the gasifier decreases, due to the heat transfer with the cold biomass entering the unit. The role of heterogeneous and secondary gas phase reactions is well evident, not only in the definition of temperature profiles, but also in the proper characterization of bio-syngas composition, including hydrocarbon species, residual tars and organic volatile components.

This comprehensive model, beside the design and operation of the gasifier, can also support the study of transient conditions checking in real-time that the biomass temperature profile remains within the threshold values. Actually, the model allows to infer certain unavailable measurements, to replace multiple thermocouples and to provide reliable continuous temperature profiles so as to monitor and manage some key-parameters and maintain them within reasonable operational ranges, predicting the behavior and performances of the overall gasifier.

4.5. *Traveling grate combustion of biomass*

The last application example deals with a traveling grate combustor where a bed of biomass particles is progressively dried, devolatilized and burnt as reported in Fig. 8 (Ranzi et al., 2011). Volatile components released by the biomass traveling on the grate are involved in secondary gas-phase decomposition and combustion reactions over the solid bed, in the freeboard volume. Then, flue gases leave the freeboard and enter the boiler for steam/power generation. This combustor is rather complex to model since it involves all the previous issues and a gas-phase combustion in the freeboard, where the attention must be also focused on the effective mixing of primary and secondary air with the volatile species in order to improve combustion and minimize pollutant emissions.

Here, the fixed bed of biomass particles is considered as successive stacks of several reactor layers (Fig. 8). Again, each reactor layer is composed by spherical biomass particles that exchange mass and heat with a perfectly stirred gas phase. The stacks of elementary layers move on the grate with fixed velocity and this velocity determines the effective residence time of the solid particles inside the combustor unit. During the fuel

Please cite this article as: Ranzi, E., et al., Kinetic modeling of the thermal degradation and combustion of biomass. Chem. Eng. Sci. (2013), http://dx.doi.org/10.1016/j.ces.2013.08.014

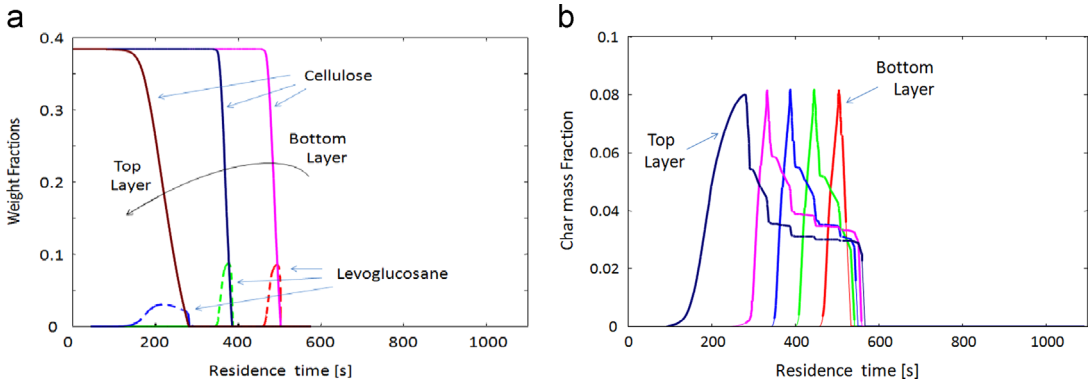

Fig. 9. (a) Cellulose devolatilization and LVG formation in the different reactor layers. (b) Char formation and combustion in the different reactor layers.

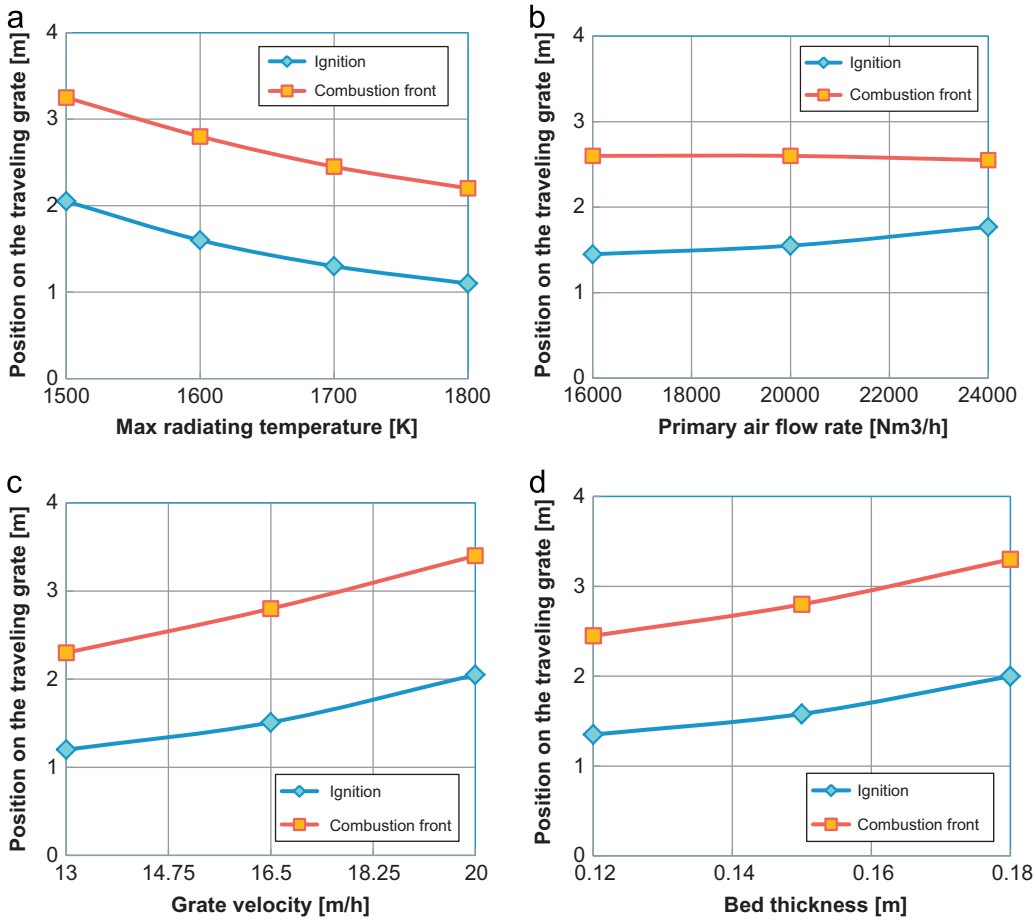

Fig. 10. Control parameters of traveling grate biomass combustor.

conversion, the size, density, and porosity of the individual particles change, due to drying, devolatilization and char gasification and combustion. These variations and the shrinking of the reacting system are taken into account at the particle and reactor scale. Finally, the freeboard gas phase section requires the boundary conditions to properly close the balance equations on the overall reactor.

Fig. 9a shows the cellulose devolatilization and the formation of levoglucosan versus the residence time along the grate. Due to the wall radiating heat, the top reactor layer is the first to heat and pyrolyze, while the bottom layer takes more time to decompose. On the contrary, Fig. 9b shows that the combustion reactions of the residual char follow the reverse order. Due to the limited availability of the oxygen in the primary air, there is initially the combustion of the char in the bottom layer and only then the combustion of the char in the top layer can be completed. These figures are only a couple of examples of the detailed results the model is able to provide. This mathematical model has been tested and validated in comparison with experimental data from an industrial biomass combustor of 12 MW designed by Garioni Naval and operating in Belgium.

While a more complete description of this model and relating results are reported elsewhere (Ranzi et al., 2011), here the main interest is to show the viable application of this modeling approach also to the control of industrial scale combustors. This model allows not only to monitor the performance of the grate

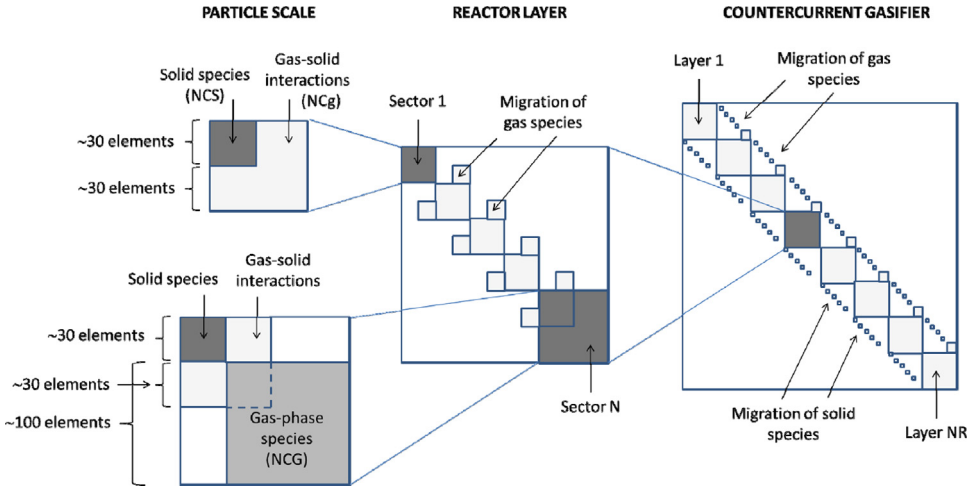

Fig. A1. Qualitative structure of the Jacobian matrix of this multi-scale system (countercurrent gasifier).

combustor, but also to control it by manipulating the operating variables depending on biomass characteristics within their own operability range around the nominal operating conditions. The main control parameters are the grate velocity, thickness of biomass bed, radiating temperature, and primary/secondary air flow rate. The proper manipulation of these control variables ensures the biomass devolatilization, the char conversion and the complete combustion in the freeboard, controlling in this way the emissions in flue gases as well as carbon content in the residual ashes. The sensitivity analysis for the complete decoupling of control parameters is given in Fig. 10.

The effective radiating temperature is an average of wall and flame temperature. Fig. 10a shows the effect of this temperature on the ignition point and combustion front along the traveling grate. The higher radiating temperature leads to the ignition point closer to the biomass inlet. Similarly, the combustion front appears anticipated, while the width of the front is preserved. The width is $\sim$1 m and it mainly depends on the primary air, as shown in Fig. 10b. Thus, the increase of primary air allows to delay the ignition point, while the higher amount of oxygen supplied reduces the width of the combustion front. The variation of grate velocity (Fig. 10c) is analyzed with the corresponding variation of primary and secondary air to maintain the combustion stoichiometry. This corresponds to vary the whole boiler capacity. The increase in grate velocity and capacity, moves the ignition and combustion front towards the end of the grate, thus limiting the combustor operability. Finally, the effect of bed thickness on the grate is reported in Fig. 10d maintaining the same grate velocity. At the same combustion conditions, it is possible to highlight the limiting bed thickness.

5. Conclusions

This paper analyses the pyrolysis, gasification, and combustion of biomass in terms of a multi-component, multi-phase, multi-scale system. This challenging problem requires several assumptions and simplifications at different levels: description of biomass through a mixture of reference components, proper lumping of solid, gas and tar species in order to reduce the complexity of both the biomass and the gas-phase kinetic schemes, and finally the coupling of a particle model with the kinetic schemes. Detailed descriptions of the kinetic schemes, particle and reactor models are reported aiming at providing the reader with the useful insights for reproducing the whole set of results. Applications at the particle scale show a possible overshooting effect of internal temperature for the pyrolysis of relatively thick biomass particle. Further examples handle the issues relating to the start-up operation of autothermal systems, and demonstrate the possibility of gasification and combustion regimes according to particle geometry and operating conditions. At the reactor scale, the predictions of thermal profile inside the biomass bed of the gasifier and of the ignition and combustion front inside the traveling grate combustor show the model potentialities. Furthermore, sensitivity analysis and very foundations of process dynamics and control are provided for a traveling grate biomass combustor. As already mentioned, these application examples show the flexibility and possibilities as well as the limitations of the proposed approach in the design, simulation, and control of biomass pyrolysis, gasification, and combustion units. Lumped kinetic models, both for biomass devolatilization and for the secondary gas phase reactions, are always susceptible to improvements and extensions on the basis of new available data. Nevertheless, it seems relevant to observe that the comprehensive model of biomass pyrolysis, gasification, and combustion is already able to provide a wide range of useful predictions in a feasible way.

Acknowledgments

This research work was partially supported by the Italian Government MSE/CNR (Clean Coal Project). Authors gratefully acknowledge the useful suggestions and comments of Prof. T. Faravelli and A. Frassoldati.

Appendix A. Jacobian structure and numerical methods

According to the multi-scale nature of the mathematical model, the resulting Jacobian has an embedded highly-sparse and large-scale structure with diagonal-blocks and upper and lower bands, as schematically reported in Fig. A1.

Two different matrices are adopted to first characterize the biomass particle. The first is a $(NCS+NCg+1)\times(NCS+NCg+1)$ dense matrix accounting for all the solid species *NCS* as well as only the gas species *NCg* ($NCg<NCG$) that interact with the solid. It accounts for the intra-particle solid and gas-solid evolution within each sector of the particle. Only the external sector N interacts with all the *NCG* gas species. In order to give an idea of the dimension of this problem, let's assume 30 solid species, 100 gas species, and only 30 gas species really interacting with the solid matrix.

The second is a $(NCS+NCG+1)\times(NCS+NCG+1)$ partially structured matrix, of the order of 130×130, accounting for all

the solid and gas species in the external sector. Biomass devolatilization, heterogeneous reactions and secondary gas phase reactions are accounted for.

At the scale of the reactor layer, since the solid species are not diffusing, the upper and lower bands involve only gas species and *NCg* (30) is the size of the band block. Both the bands are present since gas species diffuse inside the particle. Finally, the external sector accounts for all the gas species. The dimension of this matrix easily becomes 500×500.

At the reactor scale, i.e. at the scale of the cascade of reactor layers, each layer interacts with the gas stream coming from the upper or lower layer, depending on the countercurrent or the concurrent configuration. Similarly, there is the migration of the solid variables across the different layers. Thus, the numerical structure of the Jacobian for the reactor scale assumes a diagonal-block structure with asymmetric bands. Referring to a countercurrent biomass gasifier (Section 4.4), the lower band represents the solid particles that migrate towards the lower layers while the upper band represents the gas species rising the biomass bed. The asymmetry of lower and upper bands comes from the larger number of gas species ($NCG > NCS$).

By assuming 5–10 sectors to discretize the particles and a similar number of reactor layers, the number of balance equations easily overcomes 5000 and leads to numerical difficulties. Very often, it is possible to re-order the Jacobian structure so as to achieve a diagonally dominant structure that allows to reduce the computational effort. Ordinary differential and differential-algebraic equation (ODE and DAE) system solvers belonging to BzzMath library (Buzzi-Ferraris and Manenti, 2012; Manenti et al., 2009) are adopted. Dsmoke and OpenSmoke codes are used for calculations of gas-phase ideal reactors (Cuoci et al., 2013). Stiffness is the principal responsible for the computation effort, which may vary from a few minutes to some hours, depending on the kinetic scheme and the adopted discretization. The computation time versus the problem size varies with a power of about 2.5.

Appendix A. Supporting information

Supplementary data associated with this article can be found in the online version at http://dx.doi.org/10.1016/j.ces.2013.08.014.

References

Bennadji, H., Smith, K., Shabangu, S., Fisher, E., 2012. Experimental and Modeling Study of Woody Biomass Pyrolysis Under Low Temperature Conditions. AIChE Annual Meeting, International Congress on Energy (ICE), Pittsburgh, PA, USA.

Blondeau, J., Jeanmart, H., 2012. Biomass pyrolysis at high temperatures: prediction of gaseous species yields from an anistropic particle. Biomass and Bioenergy 41, 107–121.

Buzzi-Ferraris, G., Manenti, F., 2010. A combination of parallel computing and object-oriented programming to improve optimizer robustness and efficiency. Computer Aided Chemical Engineering 28, 337–342.

Buzzi-Ferraris, G., Manenti, F., 2012. BzzMath: library overview and recent advances in numerical methods. Computer Aided Chemical Engineering 30, 1312–1316.

Carstensen, H.H., Dean, A.M., 2010. Development of detailed kinetic models for the thermal conversion of biomass via first principle methods and rate estimation rules. Computational Modeling in Lignocellulosic Biofuel Production, ACS Symposium Series 1052, 201–243.

Cuoci, A., Frassoldati, A., Faravelli, T., Ranzi, E., 2013. A computational tool for the detailed kinetic modeling of laminar flames: application to C_2H_4/CH_4 coflow flames. Combustion and Flame 160, 870–886.

Dente, M., Ranzi, E., Goossens, A.G., 1979. Detailed prediction of olefin yields from hydrocarbon pyrolysis through a fundamental simulation model (SPYRO). Computers and Chemical Engineering 3, 61–75.

Di Blasi, C., 1993. Modeling and simulation of combustion processes of charring and non-charring solid fuels. Progress in Energy and Combustion Science 19, 71–104.

Di Blasi, C., 2008. Modeling chemical and physical processes of wood and biomass pyrolysis. Progress in Energy and Combustion Science 34, 47–90.

Faravelli, T., Frassoldati, A., Migliavacca, G., Ranzi, E., 2010. Detailed kinetic modeling of the thermal degradation of lignins. Biomass and Bioenergy 34, 290–301.

Frigerio, S., Thunman, H., Leckner, B., Hermansson, S., 2008. Estimation of gas phase mixing in packed beds. Combustion and Flame 153, 137–148.

Gauthier, G., Melkior, T., Salvador, S., Corbetta, M., Frassoldati, A., Pierucci, S., et al., 2013. Pyrolysis of thick biomass particles: experimental and kinetic modeling. Chemical Engineering Transactions 32, 601–606.

Groeneveld, M.J., Van Swaaij, W.P.M., 1980. Gasification of char particles with CO_2 and H_2O. Chemical Engineering Science 35, 307–313.

Kashiwagi, T., Nambu, H., 1992. Global kinetic constants for thermal oxidative degradation of a cellulosic paper. Combustion and Flame 88, 345–368.

Lédé, J., 2012. Cellulose pyrolysis kinetics: an historical review on the existence and role of intermediate active cellulose. Journal of Analytical and Applied Pyrolysis 94, 17–32.

Lewis, A.D., Fletcher, T.H., 2013. Prediction of sawdust pyrolysis yields from a flat-flame burner using the CPD model. Energy and Fuels 27, 942–953.

Manenti, F., Dones, I., Buzzi-Ferraris, G., Preisig, H.A., 2009. Efficient numerical solver for partially structured differential and algebraic equation systems. Industrial and Engineering Chemistry Research 48, 9979–9984.

Mettler, M.S., Vlachos, D.G., Dauenhauer, P.J., 2012. Top ten fundamental challenges of biomass pyrolysis for biofuels. Energy and Environmental Science 5, 7797–7809.

Miller, R.S., Bellan, J., 1997. A generalized biomass pyrolysis model based on superimposed cellulose, hemicellulose and lignin kinetics. Combustion Science and Technology 126, 97–137.

Milosavljevic, I., Oja, V., Suuberg, E.M., 1996. Thermal effects in cellulose pyrolysis: relationship to char formation processes. Industrial and Engineering Chemistry Research 35, 653–666.

Norinaga, K., Shoji, T., Kudo, S., Hayashi, J., 2013. Detailed chemical kinetic modelling of vapour-phase cracking of multi-component molecular mixtures derived from the fast pyrolysis of cellulose. Fuel 103, 141–150.

Park, W.C., Atreya, A., Baum, H.R., 2010. Experimental and theoretical investigation of heat and mass transfer processes during wood pyrolysis. Combustion and Flame 157, 481–494.

Pierucci, S., Ranzi, E., 2008. A general mathematical model for a moving bed gasifier. In: Braunschweig, B., Joulia, X. (Eds.), 18th European Symposium on Computer Aided Process Engineering. Elsevier Science Bv, Amsterdam, pp. 901–906.

Ranz, W.E., Marshall, W.R., 1952. Evaporation from drops, part I. Chemical Engineering Progress 48, 141–146.

Ranzi, E., Cuoci, A., Faravelli, T., Frassoldati, A., Migliavacca, G., Pierucci, S., et al., 2008. Chemical kinetics of biomass pyrolysis. Energy and Fuels 22, 4292–4300.

Ranzi, E., Frassoldati, A., Grana, R., Cuoci, A., Faravelli, T., Kelley, A.P., et al., 2012. Hierarchical and comparative kinetic modeling of laminar flame speeds of hydrocarbon and oxygenated fuels. Progress in Energy and Combustion Science 38, 468–501.

Ranzi, E., Pierucci, S., Aliprandi, P.C., Stringa, S., 2011. Comprehensive and detailed kinetic model of a traveling grate combustor of biomass. Energy and Fuels 25, 4195–4205.

Ranzi, E., Sogaro, A., Gaffuri, P., Pennati, G., Westbrook, C.K., Pitz, W.J., 1994. New comprehensive reaction-mechanism for combustion of hydrocarbon fuels. Combustion and Flame 99, 201–211.

Saggese, C., Cuoci, A., Frassoldati, A., Faravelli, T., Ranzi, E., 2013. Gas Phase Kinetics of Volatiles from Biomass Pyrolysis. Note II: Furan, 2-methyl-furan, and 2,5-dimethyl-furan. XXXVI Meeting of the Italian Section of the Combustion Institute.

Seshadri, V., Westmoreland, P.R., 2012. Concerted reactions and mechanism of glucose pyrolysis and implications for cellulose kinetics. Journal of Physical Chemistry A 116, 11997–12013.

Sommariva, S., Grana, R., Maffei, T., Pierucci, S., Ranzi, E., 2011. A kinetic approach to the mathematical model of fixed bed gasifiers. Computers and Chemical Engineering 35, 928–935.

Tognotti, L., Longwell, J.P., Sarofim, A.F., 1991. The products of the high temperature oxidation of a single char particle in an electrodynamic balance. Symposium (International) on Combustion 23, 1207–1213.

Vinu, R., Broadbelt, L.J., 2012. A mechanistic model of fast pyrolysis of glucose-based carbohydrates to predict bio-oil composition. Energy and Environmental Science 5.12, 9808–9826.

Weng, J., Jia, L., Wang, Y., Sun, S., Tang, X., Zhou, Z., et al., 2013. Pyrolysis study of poplar biomass by tunable synchrotron vacuum ultraviolet photoionization mass spectrometry. Proceedings of the Combustion Institute 34, 2347–2354.

Williams, A., Jones, J.M., Ma, L., Pourkashanian, M., 2012. Pollutants from the combustion of solid biomass fuels. Progress in Energy and Combustion Science 38, 113–137.